Quasi-two-dimensional relativistic fermions probed by dHvA quantum oscillations in $LuSn_2$

Yanglin Zhu[1], Jin Hu[2,3], David Graf[4], Xin Gui[5], Weiwei Xie[6] and Zhiqiang Mao[1*]

[1] Department of Physics, Pennsylvania State University, University Park, PA, 16802

[2] Department of Physics, University of Arkansas, Fayetteville, AR, 72701

[3] Institute for Nanoscience and Engineering, University of Arkansas, Fayetteville, AR 72701

[4] National High Magnetic Field Laboratory, Tallahassee, FL 32310

[5] Department of Chemistry, Louisiana State University, Baton Rouge LA 70803

[6] Department of Chemistry and Chemical Biology, Rutgers University, Piscataway NJ 08854

Abstract

We report de Haas–van Alphen (dHvA) quantum oscillation studies on a layered compound $LuSn_2$. Through the analyses of the dHvA oscillation data, we find this material has several 3D bands and one quasi-2D band hosting relativistic fermions. Compared to previously reported dHvA oscitations in YSn_2, the oscillation component arising from the quasi-2D band is significantly enhanced. From structural analyses using single crystal X-ray diffraction, we find the distorted Sn-square net layer is less corrugated than YSn_2, which accounts for the enhancement of two-dimensionality of the relativistic fermions created in this layer. This result suggests that the dimensionality of relativistic band in $RESn_2$ (RE=rare earth) can be tuned by electronegativity of RE. Moreover, we also find the 3D relativistic bands are pushed closer to the Fermi level with respect to YSn_2 due to enhanced spin-orbital coupling. These findings imply $RESn_2$ can be an

interesting platform for seeking new topological states via the tuning of electronegativity, spin-orbital coupling and magnetism.

* Email: zim1@psu.edu

I. INTRODUCTION

3D topological materials, including Dirac [1–6], Weyl [7–14], and nodal-line semimetals [15–17], possess linear band crossing points, *i.e.*, Dirac/Weyl points, in their bulk electronic band structure. The quasiparticles excited near the Dirac or Weyl points can be described as relativistic fermions, which can give rise to striking exotic properties, such as large magnetoresistance [18–24], high transport mobility [18,25] and chiral anomaly [24,26,27]. Among current 3D topological materials, one class of materials feature layered structures and their topological states are created by 2D square lattices or distorted square lattices formed by group IV or V elements. The examples include ATX_2 (A=Ca, Sr, Ba, or rare earth, T=Mn, Zn or Ag; X=Bi or Sb) [28–38] and WHM (W = Zr, Hf, or rare-earth elements; H = Si, Ge, Sn, Sb; and M = S, Se, Te) [39–48]. A variety of unique topological semimetal states has been observed in these materials, such as the anisotropic Dirac cone state in $SrMnBi_2$ [28], the nodal-line and 2D non-symmorphic Dirac states in ZrSi(S/Se/Te) [39,40,42,49–53], the Dirac state with spin-valley locking in $BaMnSb_2$ [54]. Moreover, magnetism can also be present in some members of the ATX_2 and WHM families, in which the interplay between magnetism and non-trivial bands may generate even more exotic states, e.g. the time-reversal symmetry breaking Weyl state in $YbMnBi_2$ [38], the bulk quantum Hall Effect (QHE) in $EuMnBi_2$ [55], magnetically tuned Dirac state in $SrMnSb_2$ [33], and tunable Weyl and Dirac states in CeSbTe [44],

In addition to Si, Sb, and Bi square lattices, square or distorted square lattice of Sn has also been demonstrated to generate topological states. Examples include ZrSnTe [56,48] and YSn_2 [57]. ZrSnTe belongs to the WHM family with Sn square net that creates topological surface states [56], whereas the Sn square lattice in YSn_2 is distorted and forms non-centrosymmetric orthorhombic structure. Earlier de Haas-van Alphen (dHvA) quantum oscillation studies on

YSn_2 [57] revealed multiple topological non-trivial bands, including a 3D band hosting a possible tunable Weyl state and a quasi-2D band. While the 3D Weyl band is predicted theoretically, the origin of the quasi-2D band remains elusive [57].

In this work, we have performed dHvA quantum oscillation studies on $LuSn_2$. Though it shares a similar structure with YSn_2, the relatively larger electronegativity and stronger SOC of Lu would possibility affect its electronic states. In our experiments, we observed very strong dHvA oscillations in $LuSn_2$ single crystals. Interestingly, the oscillation component arising from the quasi-2D band is much stronger than that due to the 3D bands, in stark contrast with the scenario seen in YSn_2 where the oscillation component from the quasi-2D band is much weaker than that of the 3D band [57]. Additionally, compared to YSn_2, the 3D non-trivial bands in $LuSn_2$ are pushed closer to the Fermi level. From single crystal structural analyses, we find the Sn square lattice is much less distorted than that of YSn_2, thus enhancing the two-dimensionality of the bands arising from the Sn 2D layer. This explains the significant enhancement of the dHvA oscillations originating from the quasi-2D band. These results not only demonstrate an effective pathway of non-trivial band tuning through controlling electronegativity and SOC, but also suggest $RESn_2$ (RE=rare earth) could be an interesting platform for seeking novel topological states through tuning of electronegativity, SOC and magnetism.

II. METHODS

The $LuSn_2$ single crystals were synthesized using a metal flux method. The Lu pieces and Sn lumps with the molar ratio of 1:10 were loaded in an Al_2O_3 crucible and sealed in a quartz tube under high vacuum. The mixture was heated to 1050 °C, held at this temperature for 48 hours for homogeneous melting, and slowly cooled down to 750 °C at a rate of 2 °C per hour. The plate-like single crystals with silver luster (see inset of Fig. 1e) can be obtained after removing the excess Sn

flux by centrifugation. The composition of the grown crystals was confirmed to be approximately stoichiometric using an energy dispersive X-ray spectrometer (EDS). The excellent crystallization of the single crystals was verified by the sharp (0*K*0) X-ray diffraction peaks (Fig. 1d). The crystal structure of the grown crystals was characterized using single crystal X-ray diffraction, as presented below. The magnetization was measured using a SQUID magnetometer (Quantum Design), and the magnetic torque measurements were carried out at the National High Magnetic Field Lab (NHMFL) in Tallahassee using a cantilever torque magnetometer.

III. RESULTS AND DISCUSSIONS

A. Structure determination of $LuSn_2$

Single crystal X-ray diffraction data were collected at 200 K, 150 K and 115 K on a Bruker Apex II diffractometer with Mo radiation Kα_1 (λ=0.71073 Å) and refined with the SHELEXTL package. The best refinement of the single-crystal X-ray spectra on $LuSn_2$ indicates the structure with a space group *Cmcm* which is consistent with the previous report [58]. The details of structural parameters are summarized in Table I. Similar to YSn_2, the structure of $LuSn_2$ can be viewed as stacking of [$Lu_2^{3+}Sn_2^{2-}$] blocks and Sn planes. The Sn square net in YSn_2 is distorted with the bonding angles slightly deviating from 90° (88.68° and 91.27°). In contrast, in $LuSn_2$, the bonding angle between the Sn-Sn bonds of the Sn square net is closer to 90°, i.e., 89.06° and 90.91°, as shown in the top-view of the distorted Sn square net (Fig. 1b). From the side-view of the square plane (Fig. 1c), we find that the Sn atoms form 2D planes with very small corrugation. The relative displacement Δd of Sn atoms of the 2D Sn layer along the *b*-axis is 0.048 Å in $LuSn_2$ (Fig. 1c), smaller than that in YSn_2 (0.061 Å). This suggests that the Sn square net in $LuSn_2$ is less corrugated than that in YSn_2. This is consistent with our dHvA oscillation observations (see below), which suggests that Sn square lattice hosting the topological state becomes more 2D-like in $LuSn_2$.

B. Relativistic fermions in $LuSn_2$ probed by dHvA oscillations

Signatures of topological relativistic fermions in $LuSn_2$, including light effective mass, high mobility, and non-trivial Berry phase, have been extracted from our dHvA quantum oscillation studies on single crystals. We have observed clear dHvA oscillations in the isothermal magnetization measurements using a SQUID magnetometer. As shown in Fig. 1e, when the magnetic field was applied along the out-of-plane direction (i.e., $B \parallel b$-axis), the magnetization at 1.8K starts to show oscillations above 3T, and the oscillations remain discernible up to 25K. Such oscillations become more conspicuous after removing the non-oscillation background, as shown in Fig. 2a. A single oscillation frequency of 70 T (denoted by F_{β}^{Lu} below) can be extracted from the Fast Fourier transform (FFT) analyses, as shown in the inset of Fig. 2b. For in-plane magnetic field, however, no oscillation can be probed up to 7T (the highest field which can be achieved in our SQUID), consistent with the 2D-like electronic structure expected for layered materials. This is also confirmed by Fermi surface morphology revealed by the angular dependence of dHvA oscillation measurements, as will be discussed below.

We can extract further information about the relativistic fermions from analyses of dHvA oscillations. The dHvA oscillations can be described by the Lifshitz-Kosevich (LK) formula [59,60], with a Berry phase being taken into account:

$$\Delta M \propto -B^{1/2} R_T R_D R_S \sin[2\pi(\frac{F}{B} + \gamma - \delta)] \qquad (1),$$

Where $R_T = \alpha T m^*/[Bm_0 \sinh(\alpha T m^*/Bm_0)]$, $R_D = \exp(-\alpha T_D m^*/Bm_0)$ and $R_S = \cos(\pi g m^*/2m_0)$. The α is a constant which equals $(2\pi^2 k_B m_0)/(\hbar e)$ and T_D is the Dingle temperature. The $\gamma - \delta$ is the phase

factor, in which $\gamma = \frac{1}{2} - \frac{\phi_B}{2\pi}$ and ϕ_B is Berry phase. The phase shift δ is determined by the dimensionality of the Fermi surface (FS); δ equals 0 and ±1/8 for 2D and 3D cases, respectively, with the sign depending on whether the probed extreme cross-section area of the FS is maximal (−) or minimal (+).

From the LK formula, the effective mass m^* of quasi-particles can be estimated from the fit of the temperature dependence of the oscillation amplitude by the thermal damping factor R_T. As shown in Fig. 2b which plots the temperature dependence of the FFT oscillation amplitude, the fit yields a small effective mass, ~0.069 m_0 (m_0, free electron mass). With the known parameters of effective masses and oscillation frequency, we have further fitted the dHvA oscillation patterns at 1.8 K to the LK-formula, as shown in Fig. 2c. From the fit, we have exacted the Dingle temperature of 10 K, from which the quantum mobility μ_q [$= e\hbar/(m^* 2\pi k_B T_D)$] is estimated to be 3102 $cm^2V^{-1}s^{-1}$.

Besides the light effective mass and high quantum mobility, the non-trivial Berry phase Φ_B is also extracted by LK formula fitting and Landau level (LL) index fan diagram, as shown in Fig. 2c and d. Through the above LK-formula fitting (Fig. 2c), the extracted phase factors is $\gamma - \delta$ = 0.048, from which the Berry phase of $(0.452\text{-}\delta) \times 2\pi$ can be derived. The measurements of angular dependence of dHvA oscillations presented later indicates that the band with the oscillation frequency of F_β^{Lu} exhibits 2D characteristics, implying that δ should be taken as 0 and thus the Berry phase is 0.904 π, close to the ideal value of π for non-trivial topological bands. To further verify the Berry phase, we also performed the LL index Fan diagram fitting, as shown in Fig 2d. In general, for a system exhibiting quantum oscillations with a single frequency, the Berry phase can be determined from the LL index fan diagram, i.e., the plot of the Landau indices *n* versus the

inverse magnetic field $1/B$, and the linear extrapolation should intercept the n axis at $\frac{\phi_B}{2\pi} - \delta$.

According to customary practice, integer LL indices should be assigned when the density of state at the Fermi level DOS(E_F) reaches a minimum. For dHvA oscillations, the oscillatory susceptibility χ is proportional to the oscillatory DOS(E_F). Given that χ is the derivative of magnetization M, the minima of the magnetization and susceptibility are shifted by $\pi/2$. Therefore, when the oscillations of magnetization are used for determining the LL fan diagram, the minima of M should be assigned with $n - 1/4$ (where n is an integer number) [42,60,61]. Through this approach, the intercept to the n axis is determined to be 0.51; thus the Berry phase is 1.02 π, which is in good agreement with the value determined from the LK-fitting.

Although the dHvA oscillations measured in low magnetic field range only revealed a single frequency, it may not indicate that the $LuSn_2$ is single band system. To obtain more comprehensive information on electronic band structure, we have further performed magnetic torque measurements up to 31T on $LuSn_2$ at the NHMFL. It is worth pointing out that the torque signal is expected to vanish when the magnetic field is exactly aligned along the out-of-plane (B || b axis) and in plane (B || ac plane) direction. To obtain finite torque signal, we performed the magnetic torque measurements with field nearly along the b axis and ac plane, which are denoted by B || b' and B || ac' respectively. We indeed observed multiple oscillation frequencies in high field torque measurements. As shown in Fig. 3a, for B || b', at T = 1.8K, the oscillations exhibit single frequency at low field, and two additional high frequencies components start to appear for B > 12T. The FFT analyses (inset of Fig. 3b) reveal three frequencies: F_{β}^{Lu} =70T (i.e. the one probed by the SQUID magnetometer), and two additional higher frequencies $F_{\gamma}^{Lu} = 422$ T and $F_{\theta}^{Lu} = 511$ T. The fit of the temperature dependence of FFT amplitudes to the R_T yields an

effective electron mass of 0.053 m_0 for the β-band, as shown in Fig. 3b. This value is smaller than that obtained from the SQUID magnetometer measurements noted above (0.069 m_0). Such a discrepancy is likely caused by the fewer data points for torque measurements. For the bands with high frequency F_{γ}^{Lu} and F_{θ}^{Lu}, we obtained comparable light effective masses, i.e. m^*_{γ}=0.068 m_0 and m^*_{θ}=0.072m_0.

To further evaluate the properties of quasiparticles hosted by the β-, γ- and θ-bands, we have performed the LK-fit for the T = 1.8K oscillatory torque components obtained by subtracting the non-oscillating background. To minimize fitting parameters, we have separated the F_{β}^{Lu} component from the F_{γ}^{Lu} and F_{θ}^{Lu} components. The fit shown in Fig. 3c is made for the single F_{β}^{Lu} component. The LK-fit yields Berry phase to be 0.996π, which is consistent with the value extracted from the dHvA oscillation pattern measured by the SQUID magnetometer. This result further supports the non-trivial topological nature of the β-band in $LuSn_2$. For the high-frequency components (F_{γ}^{Lu} and F_{θ}^{Lu}) shown in Fig. 3d, the oscillation pattern at T=1.8 K can be fitted well by the two-band LK model. From this fit, we obtained non-trivial Berry phases, (0.598$\pm$ 0.25)π and (1.038$\pm$ 0.25)π for the γ- and θ-bands, as listed in Table II. As shown below, the γ- and θ-bands display the 3D nature so that δ is taken as $\pm$1/8 in their Berry phase's estimate. This result suggests that all three bands probed by the dHvA oscillations host relativistic fermions. Other signatures of relativistic fermions, such as high quantum mobility, are also revealed by LK fits, as summarized in Table II.

In addition to elucidating the non-trivial nature of multiple bands in $LuSn_2$, we also investigated the Fermi surface morphology by measuring the angular dependences of the quantum oscillations. In Fig. 4, we present two sets of angular dependences of quantum oscillation, which

are measured by the SQUID magnetometer (Fig 4a) and magnetic torque (Fig 4c) respectively. The F_{β}^{Lu} oscillation component is probed in both magnetization and torque measurements. The backgrounds have been subtracted for the data presented in Fig. 4a and 4c. As shown in Fig. 4a, for $B \parallel b'$, the low field oscillation pattern obtained by the SQUID magnetometer only contains the single frequency F_{β}^{Lu}. When the field starts to rotate away from the b axis (i.e., toward in-plane direction), the oscillation is gradually suppressed and finally disappears at the rotation angle of $\theta >$ 44°. Such an evolution of F_{β}^{Lu} is also reproduced by the magnetic torque measurements (Fig 4c). We summarized the angular-dependent F_{β}^{Lu} in Fig. 4b, where the black hollow and solid circles represent the data measured by SQUID magnetometer and torque, respectively. The data can be well-fitted to a $1/\cos\theta$ dependence, suggesting the quasi-2D nature of the F_{β}^{Lu} band. In Fig. 4b we also include the angular dependences of the other two higher frequency branches F_{γ}^{Lu} and F_{θ}^{Lu}. Both of them are present in the full angular range up to 90°, indicating the 3D nature of these two bands.

C. Discussion

From the above dHvA oscillation analysis, we conclude that $LuSn_2$ hosts three topological-nontrivial bands, i.e., the quasi-2D β_{Lu}-band and 3D γ_{Lu}- and θ_{Lu}- bands. The properties of relativistic fermions hosted by these bands are manifested by light effective mass (0.069-0.072m_0), high quantum mobility and non-trivial Berry phase. Although these relativistic fermions' properties are similar to those of YSn_2 [57], the electronic band structure of $LuSn_2$ shows distinct characteristic, as discussed below. YSn_2 involves five non-trivial topological bands, i.e. one quasi-2D band (β_Y) and four 3D anisotropic bands (α_Y, γ_Y, θ_Y and ϕ_Y) [57]. Theory predicts that the α_Y-band hosts a new type of Weyl state caused by Rashba spin-orbital coupling. The 3D γ_Y, θ_Y and

ϕ_Y-bands probed in the dHvA oscillations are also verified in the band structure calculations. However, the quasi-2D β_Y-band was not identified in the band structure calculations, the reason of which is that the calculated band with quasi-2D character forms a Fermi surface sheet with an extremely complicated geometric shape and has strong anisotropy (Fig. 7b in ref. [57]). Although the large portion of this pocket is open, it can possibly form a small closed cyclotron orbit corresponding to the probed frequency F_β^Y at a certain k_y when the magnetic field is applied along the b-axis. But, quantitative determination of the extremal cyclotron orbit for this quasi-2D, complicated Fermi surface sheet is difficult, since it is not on a high symmetric plane. Given the structural similarity between $LuSn_2$ and YSn_2, it is reasonable to assume $LuSn_2$ shares some similarity in band structure with YSn_2. This is indeed verified by the fact that both the γ- and θ-pockets are probed in both $LuSn_2$ and YSn_2, though the size of these pockets becomes larger in $LuSn_2$. Therefore, the quasi-2D β-band of $LuSn_2$ probed in our dHvA experiments likely has similar nature with that in YSn_2, i.e. this band forms the extremely anisotropic Fermi surface.

In $LuSn_2$, while the α-band is not probed, the oscillation component due to the quasi-2D β-band is significantly enhanced as compared to YSn_2. We observed a remarkable increase in the amplitude of dHvA oscillation of the β- band, which is almost two times larger than that of the γ-band (see the inset to Fig. 3b). In contrast, the torque measurements on YSn_2 barely probed the quasi-2D β-band for $B \parallel b'$, though it is observed in magnetization measurements (see Fig. 3b in ref [57]). Such a significant enhancement of the quantum oscillation amplitude suggests that the two-dimensionality of the β-band in $LuSn_2$ is greatly increased when compared with YSn_2, since 2D bands are generally known to generate much stronger quantum oscillations than 3D bands [60,62].

The increase of the two-dimensionality of the β-band in $LuSn_2$ can be attributed to the fact that the electronegativity difference between Lu and Sn is larger than the one between Y and Sn. As noted above, YSn_2 or $LuSn_2$ is characterized by the distorted Sn2 square lattice, which is sandwiched by two (Y/Lu)Sn1 blocks, as shown in Fig. 1a. The Y atom is coordinated with six Sn1 (Sn atoms in YSn block) and four Sn2 atoms. Due to the relatively weak electronegativity of Y atom, it prefers to form the more covalent bonds with the Sn2 atoms of the square net. Such covalent bonds between Y and Sn2 atoms distort the square net of Sn2, which in turn weakens the two-dimensionality of the non-trivial state created by the distorted Sn2 square net. In contrast, in $LuSn_2$, since Lu is more electronegative than Y, Lu tends to form a more ionic bond with Sn2 than Y. The oxidation states of Lu and isolated Sn are +3 and -2; each Sn in the puckered 2D square network will be left with five valence electrons to form four equivalent Sn-Sn bonds. As such, each Sn will donate their unpaired electrons to the square network and be normal two-center two-electron (2c-2e) bonds. The observation of less puckered Sn square planar with shorter Sn-Sn distance in $LuSn_2$ implies stronger 2c-2e bonds in $LuSn_2$, thus more localized bonds in Sn square planar. In other words, the Sn square lattice becomes more isolated than that in YSn_2. Therefore, the electronic bands hosted by such a square lattice naturally become more 2D-like.

Another noticeable difference between $LuSn_2$ and YSn_2 is their crystal symmetry: YSn_2 has a non-centrosymmetric orthorhombic structure with the space group of *Cmc21*, whereas $LuSn_2$ possesses a centrosymmetric orthorhombic structure (*Cmcm*). Such a crystal symmetry change leads to the absence of the 3D α-band in $LuSn_2$. However, other 3D bands, i.e. the γ- and θ-bands, survive, but they are closer to the Fermi level, as reflected in their higher dHvA frequencies. In $LuSn_2$, F_{γ}^{Lu} and F_{θ}^{Lu} are 422T and 511T respectively, much larger than those in YSn_2 (F_{γ}^{Y} =386T, F_{θ}^{Y}=465T). The charge carriers hosted by the γ- and θ-bands in $LuSn_2$, display heavier effective

mass (m^*_γ=0.068 m_0 and m^*_θ=0.072 m_0) and much lower quantum mobility ($\mu_{q,\gamma}$ = 401cm^2/Vs, $\mu_{q,\theta}$ = 240 cm^2/Vs) as compared with YSn_2 (m^*_γ= 0.023m_0 and m^*_θ = 0.038m_0; $\mu_{q,\gamma}$ = 767 and $\mu_{q,\theta}$ = 891 cm^2/Vs) [57]. We believe the 3D γ- and θ-bands should be generated by the p-orbital of Sn1 atoms in $Lu_2^{3+}Sn_2^2$ block, which are likely affected by the stronger SOC introduced by Lu.

IV. CONCLUSION

In summary, we have synthesized single crystals of $LuSn_2$, characterized its crystal structure using single-crystal XRD and investigated its dHvA oscillations. We find that the Sn square net layer of $LuSn_2$ is less distorted than YSn_2. We observed strong dHvA oscillations in this material. From the analyses of the dHvA oscillation data, we have demonstrated that $LuSn_2$ has multiple bands hosting relativistic fermions, including two 3D bands and one quasi-2D band. Through comparison with YSn_2, we find the electronic band structure of $LuSn_2$ exhibits distinct signatures due to the enhanced electronegativity and SOC of Lu. The two-dimensionality of the β-band is significantly enhanced in $LuSn_2$ than that in YSn_2, which can be attributed to the fact that large electronegativity of Lu causes less distortion of the Sn square net. These results indicate that, in the $RESn_2$ (RE=rare-earth) system, the variation of RE atom could affect the nature of 2D square net formed by Sn atoms, which could tune the topological properties of the bands generated by the Sn 2D square lattice.

ACKNOWLEDGEMENTS

This work is supported by the US National Science Foundation under grants DMR 1832031 and 1917579. A portion of this work was performed at the National High Magnetic Field Laboratory, which is supported by National Science Foundation Cooperative Agreement No. DMR-1644779

and the State of Florida. Y.L.Z acknowledge partial financial support from the National Science Foundation through the Penn State 2D Crystal Consortium-Materials Innovation Platform (2DCC-MIP) under NSF cooperative agreement DMR-1539916. W. X. acknowledges the support from NSF-DMR-1944965.

References

[1] Z. Wang, Y. Sun, X.-Q. Chen, C. Franchini, G. Xu, H. Weng, X. Dai, and Z. Fang, Phys. Rev. B **85**, 195320 (2012).
[2] Z. K. Liu, B. Zhou, Y. Zhang, Z. J. Wang, H. M. Weng, D. Prabhakaran, S.-K. Mo, Z. X. Shen, Z. Fang, X. Dai, and others, Science **343**, 864 (2014).
[3] Z. Wang, H. Weng, Q. Wu, X. Dai, and Z. Fang, Phys. Rev. B **88**, 125427 (2013).
[4] Z. K. Liu, J. Jiang, B. Zhou, Z. J. Wang, Y. Zhang, H. M. Weng, D. Prabhakaran, S. K. Mo, H. Peng, P. Dudin, and others, Nat. Mater. **13**, 677 (2014).
[5] M. Neupane, S.-Y. Xu, R. Sankar, N. Alidoust, G. Bian, C. Liu, I. Belopolski, T.-R. Chang, H.-T. Jeng, H. Lin, and others, Nat. Commun. **5**, (2014).
[6] S. Borisenko, Q. Gibson, D. Evtushinsky, V. Zabolotnyy, B. Büchner, and R. J. Cava, Phys. Rev. Lett. **113**, 027603 (2014).

[7] S.-M. Huang, S.-Y. Xu, I. Belopolski, C.-C. Lee, G. Chang, B. Wang, N. Alidoust, G. Bian, M. Neupane, C. Zhang, S. Jia, A. Bansil, H. Lin, and M. Z. Hasan, Nat. Commun. **6**, 7373 (2015).
[8] H. Weng, C. Fang, Z. Fang, B. A. Bernevig, and X. Dai, Phys. Rev. X **5**, 011029 (2015).
[9] S.-Y. Xu, I. Belopolski, N. Alidoust, M. Neupane, G. Bian, C. Zhang, R. Sankar, G. Chang, Z. Yuan, C.-C. Lee, and others, Science **349**, 613 (2015).
[10] B. Q. Lv, H. M. Weng, B. B. Fu, X. P. Wang, H. Miao, J. Ma, P. Richard, X. C. Huang, L. X. Zhao, G. F. Chen, Z. Fang, X. Dai, T. Qian, and H. Ding, Phys. Rev. X **5**, 031013 (2015).
[11] B. Q. Lv, N. Xu, H. M. Weng, J. Z. Ma, P. Richard, X. C. Huang, L. X. Zhao, G. F. Chen, C. E. Matt, F. Bisti, V. N. Strocov, J. Mesot, Z. Fang, X. Dai, T. Qian, M. Shi, and H. Ding, Nat. Phys. **11**, 724 (2015).
[12] L. X. Yang, Z. K. Liu, Y. Sun, H. Peng, H. F. Yang, T. Zhang, B. Zhou, Y. Zhang, Y. F. Guo, M. Rahn, D. Prabhakaran, Z. Hussain, S.-K. Mo, C. Felser, B. Yan, and Y. L. Chen, Nat. Phys. **11**, 728 (2015).
[13] S.-Y. Xu, N. Alidoust, I. Belopolski, Z. Yuan, G. Bian, T.-R. Chang, H. Zheng, V. N. Strocov, D. S. Sanchez, G. Chang, C. Zhang, D. Mou, Y. Wu, L. Huang, C.-C. Lee, S.-M. Huang, B. Wang, A. Bansil, H.-T. Jeng, T. Neupert, A. Kaminski, H. Lin, S. Jia, and M. Zahid Hasan, Nat. Phys. **11**, 748 (2015).
[14] N. Xu, H. M. Weng, B. Q. Lv, C. E. Matt, J. Park, F. Bisti, V. N. Strocov, D. Gawryluk, E. Pomjakushina, K. Conder, N. C. Plumb, M. Radovic, G. Autès, O. V. Yazyev, Z. Fang, X. Dai, T. Qian, J. Mesot, H. Ding, and M. Shi, Nat. Commun. **7**, 11006 (2016).
[15] A. A. Burkov, M. D. Hook, and L. Balents, Phys. Rev. B **84**, 235126 (2011).
[16] G. Bian, T.-R. Chang, R. Sankar, S.-Y. Xu, H. Zheng, T. Neupert, C.-K. Chiu, S.-M. Huang, G. Chang, I. Belopolski, D. S. Sanchez, M. Neupane, N. Alidoust, C. Liu, B. Wang, C.-C. Lee, H.-T. Jeng, C. Zhang, Z. Yuan, S. Jia, A. Bansil, F. Chou, H. Lin, and M. Z. Hasan, Nat. Commun. **7**, 10556 (2016).
[17] C. Fang, H. Weng, X. Dai, and Z. Fang, Chin. Phys. B **25**, 117106 (2016).
[18] T. Liang, Q. Gibson, M. N. Ali, M. Liu, R. J. Cava, and N. P. Ong, Nat. Mater. **14**, 280 (2015).
[19] J. Xiong, S. Kushwaha, J. Krizan, T. Liang, R. J. Cava, and N. P. Ong, EPL Europhys. Lett. **114**, 27002 (2016).
[20] C. Shekhar, A. K. Nayak, Y. Sun, M. Schmidt, M. Nicklas, I. Leermakers, U. Zeitler, Y. Skourski, J. Wosnitza, Z. Liu, Y. Chen, W. Schnelle, H. Borrmann, Y. Grin, C. Felser, and B. Yan, Nat. Phys. **11**, 645 (2015).
[21] N. J. Ghimire, Y. Luo, M. Neupane, D. J. Williams, E. D. Bauer, and F. Ronning, J. Phys. Condens. Matter **27**, 152201 (2015).
[22] Z. Wang, Y. Zheng, Z. Shen, Y. Lu, H. Fang, F. Sheng, Y. Zhou, X. Yang, Y. Li, C. Feng, and others, Phys. Rev. B **93**, 121112 (2016).
[23] F. Arnold, C. Shekhar, S.-C. Wu, Y. Sun, R. D. dos Reis, N. Kumar, M. Naumann, M. O. Ajeesh, M. Schmidt, A. G. Grushin, J. H. Bardarson, M. Baenitz, D. Sokolov, H. Borrmann, M. Nicklas, C. Felser, E. Hassinger, and B. Yan, Nat. Commun. **7**, 11615 (2016).
[24] X. Huang, L. Zhao, Y. Long, P. Wang, D. Chen, Z. Yang, H. Liang, M. Xue, H. Weng, Z. Fang, X. Dai, and G. Chen, Phys. Rev. X **5**, 031023 (2015).

[25] Y. Zhao, H. Liu, C. Zhang, H. Wang, J. Wang, Z. Lin, Y. Xing, H. Lu, J. Liu, Y. Wang, S. M. Brombosz, Z. Xiao, S. Jia, X. C. Xie, and J. Wang, Phys. Rev. X **5**, 031037 (2015).
[26] C.-L. Zhang, S.-Y. Xu, I. Belopolski, Z. Yuan, Z. Lin, B. Tong, G. Bian, N. Alidoust, C.-C. Lee, S.-M. Huang, T.-R. Chang, G. Chang, C.-H. Hsu, H.-T. Jeng, M. Neupane, D. S. Sanchez, H. Zheng, J. Wang, H. Lin, C. Zhang, H.-Z. Lu, S.-Q. Shen, T. Neupert, M. Zahid Hasan, and S. Jia, Nat. Commun. **7**, 10735 (2016).
[27] A. A. Zyuzin and A. A. Burkov, Phys. Rev. B **86**, 115133 (2012).
[28] J. Park, G. Lee, F. Wolff-Fabris, Y. Y. Koh, M. J. Eom, Y. K. Kim, M. A. Farhan, Y. J. Jo, C. Kim, J. H. Shim, and others, Phys. Rev. Lett. **107**, 126402 (2011).
[29] Y. Feng, Z. Wang, C. Chen, Y. Shi, Z. Xie, H. Yi, A. Liang, S. He, J. He, Y. Peng, X. Liu, Y. Liu, L. Zhao, G. Liu, X. Dong, J. Zhang, C. Chen, Z. Xu, X. Dai, Z. Fang, and X. J. Zhou, Sci. Rep. **4**, 5385 (2014).
[30] K. Wang, D. Graf, L. Wang, H. Lei, S. W. Tozer, C. Petrovic, and others, Phys. Rev. B **85**, 041101 (2012).
[31] G. Lee, M. A. Farhan, J. S. Kim, and J. H. Shim, Phys. Rev. B **87**, 245104 (2013).
[32] J. B. He, Y. Fu, L. X. Zhao, H. Liang, D. Chen, Y. M. Leng, X. M. Wang, J. Li, S. Zhang, M. Q. Xue, C. H. Li, P. Zhang, Z. A. Ren, and G. F. Chen, Phys. Rev. B **95**, 045128 (2017).
[33] J. Y. Liu, J. Hu, Q. Zhang, D. Graf, H. B. Cao, S. M. A. Radmanesh, D. J. Adams, Y. L. Zhu, G. F. Cheng, X. Liu, W. A. Phelan, J. Wei, M. Jaime, F. Balakirev, D. A. Tennant, J. F. DiTusa, I. Chiorescu, L. Spinu, and Z. Q. Mao, Nat. Mater. **16**, 905 (2017).
[34] J. Liu, J. Hu, H. Cao, Y. Zhu, A. Chuang, D. Graf, D. J. Adams, S. M. A. Radmanesh, L. Spinu, I. Chiorescu, and Z. Mao, Sci. Rep. **6**, 30525 (2016).
[35] Y.-Y. Wang, S. Xu, L.-L. Sun, and T.-L. Xia, Phys. Rev. Mater. **2**, 021201 (2018).
[36] M. A. Farhan, G. Lee, and J. H. Shim, J. Phys. Condens. Matter **26**, 042201 (2014).
[37] C. Yi, S. Yang, M. Yang, L. Wang, Y. Matsushita, S. Miao, Y. Jiao, J. Cheng, Y. Li, K. Yamaura, Y. Shi, and J. Luo, Phys. Rev. B **96**, 205103 (2017).
[38] S. Borisenko, D. Evtushinsky, Q. Gibson, A. Yaresko, K. Koepernik, T. Kim, M. Ali, J. van den Brink, M. Hoesch, A. Fedorov, E. Haubold, Y. Kushnirenko, I. Soldatov, R. Schäfer, and R. J. Cava, Nat. Commun. **10**, 3424 (2019).
[39] Q. Xu, Z. Song, S. Nie, H. Weng, Z. Fang, and X. Dai, Phys. Rev. B **92**, 205310 (2015).
[40] L. M. Schoop, M. N. Ali, C. Stra\s ser, A. Topp, A. Varykhalov, D. Marchenko, V. Duppel, S. S. Parkin, B. V. Lotsch, and C. R. Ast, Nat. Commun. **7**, 11696 (2016).
[41] N. Kumar, K. Manna, Y. Qi, S.-C. Wu, L. Wang, B. Yan, C. Felser, and C. Shekhar, Phys. Rev. B **95**, 121109 (2017).
[42] J. Hu, Z. Tang, J. Liu, X. Liu, Y. Zhu, D. Graf, K. Myhro, S. Tran, C. N. Lau, J. Wei, and Z. Mao, Phys. Rev. Lett. **117**, 016602 (2016).
[43] J. Hu, Y. L. Zhu, D. Graf, Z. J. Tang, J. Y. Liu, and Z. Q. Mao, Phys. Rev. B **95**, 205134 (2017).
[44] L. M. Schoop, A. Topp, J. Lippmann, F. Orlandi, L. Müchler, M. G. Vergniory, Y. Sun, A. W. Rost, V. Duppel, M. Krivenkov, S. Sheoran, P. Manuel, A. Varykhalov, B. Yan, R. K. Kremer, C. R. Ast, and B. V. Lotsch, Sci. Adv. **4**, 2317 (2018).
[45] R. Singha, A. Pariari, B. Satpati, and P. Mandal, Phys. Rev. B **96**, 245138 (2017).
[46] R. Lou, J.-Z. Ma, Q.-N. Xu, B.-B. Fu, L.-Y. Kong, Y.-G. Shi, P. Richard, H.-M. Weng, Z. Fang, S.-S. Sun, Q. Wang, H.-C. Lei, T. Qian, H. Ding, and S.-C. Wang, Phys. Rev. B **93**, 241104 (2016).

[47] M. M. Hosen, G. Dhakal, K. Dimitri, P. Maldonado, A. Aperis, F. Kabir, C. Sims, P. Riseborough, P. M. Oppeneer, D. Kaczorowski, T. Durakiewicz, and M. Neupane, Sci. Rep. **8**, 13283 (2018).
[48] J. Hu, Y. Zhu, X. Gui, D. Graf, Z. Tang, W. Xie, and Z. Mao, Phys. Rev. B **97**, 155101 (2018).
[49] M. Neupane, I. Belopolski, M. M. Hosen, D. S. Sanchez, R. Sankar, M. Szlawska, S.-Y. Xu, K. Dimitri, N. Dhakal, P. Maldonado, P. M. Oppeneer, D. Kaczorowski, F. Chou, M. Z. Hasan, and T. Durakiewicz, Phys. Rev. B **93**, 201104 (2016).
[50] M. N. Ali, L. M. Schoop, C. Garg, J. M. Lippmann, E. Lara, B. Lotsch, and S. S. Parkin, Sci. Adv. **2**, 1601742 (2016).
[51] R. Singha, A. K. Pariari, B. Satpati, and P. Mandal, Proc. Natl. Acad. Sci. **114**, 2468 (2017).
[52] B.-B. Fu, C.-J. Yi, T.-T. Zhang, M. Caputo, J.-Z. Ma, X. Gao, B. Q. Lv, L.-Y. Kong, Y.-B. Huang, P. Richard, M. Shi, V. N. Strocov, C. Fang, H.-M. Weng, Y.-G. Shi, T. Qian, and H. Ding, Sci. Adv. **5**, 6459 (2019).
[53] H. Pan, B. Tong, J. Yu, J. Wang, D. Fu, S. Zhang, B. Wu, X. Wan, C. Zhang, X. Wang, and F. Song, Sci. Rep. **8**, 9340 (2018).
[54] J. Y. Liu, J. Yu, J. L. Ning, H. M. Yi, L. Miao, L. J. Min, Y. F. Zhao, W. Ning, K. A. Lopez, Y. L. Zhu, T. Pillsbury, Y. B. Zhang, Y. Wang, J. Hu, H. B. Cao, F. Balakirev, F. Weickert, M. Jaime, Y. Lai, K. Yang, J. W. Sun, N. Alem, V. Gopalan, C. Z. Chang, N. Samarth, C. X. Liu, R. D. Mcdonald, and Z. Q. Mao, arXiv:190706318 (2020).
[55] H. Masuda, H. Sakai, M. Tokunaga, Y. Yamasaki, A. Miyake, J. Shiogai, S. Nakamura, S. Awaji, A. Tsukazaki, H. Nakao, Y. Murakami, T. Arima, Y. Tokura, and S. Ishiwata, Sci. Adv. **2**, e1501117 (2016).
[56] R. Lou, J.-Z. Ma, Q.-N. Xu, B.-B. Fu, L.-Y. Kong, Y.-G. Shi, P. Richard, H.-M. Weng, Z. Fang, S.-S. Sun, Q. Wang, H.-C. Lei, T. Qian, H. Ding, and S.-C. Wang, Phys. Rev. B **93**, 241104 (2016).
[57] Y. Zhu, T. Zhang, J. Hu, J. Kidd, D. Graf, X. Gui, W. Xie, M. Zhu, X. Ke, H. Cao, Z. Fang, H. Weng, and Z. Mao, Phys. Rev. B **98**, 035117 (2018).
[58] Y. U. E. Cheng-Yang, Chin. J. Inorg. Chem. **11**, 025 (2011).
[59] I. M. Lifshitz and A. M. Kosevich, Sov Phys JETP **2**, 636 (1956).
[60] D. Shoenberg, *Magnetic Oscillations in Metals* (Cambridge University Press, 2009).
[61] J. Hu, S.-Y. Xu, N. Ni, and Z. Mao, Annu. Rev. Mater. Res. **49**, 207 (2019).
[62] M. V. Kartsovnik, Chem. Rev. **104**, 5737 (2004).

Table I. lattice parameters derived from single crystal XRD measurements at 200(2) K. Space group: *Cmcm* (No. 63). Lattice parameters: a = 4.3326(8) Å, b = 15.9730(3) Å, c = 4.2525(7) Å, $\alpha = \beta = \gamma = 90^{\circ}$. ($R_1$= 3.89%, wR_2 = 6.64%, Goodness of fit = 1.043 with 2357 total reflections).

Atom	Wyckoff.	Occupancy.	*x*	*y*	*z*	U_{eq}
Lu	4*a*	1	0	0.4017(1)	¼	0.0070(3)
Sn1	4*a*	1	0	0.0643(1)	¼	0.0080(4)
Sn2	4*a*	1	0	0.7514(1)	¼	0.0069(5)

Table II. Parameters derived from the analyses of dHvA oscillations for $LuSn_2$. *F*, oscillation frequency; T_D, Dingle temperature; m^*, effective mass; μ_q, quantum mobility; Φ_B, Berry phase; δ, the phase shift factor in quantum oscillations; $\delta = 0$ for a 2D FS, but ±1/8 for a 3D FS (see text).

	***F*(T)**	**Notation**	T_D**(K)**	m^*/m_0	μ_q **(cm²/Vs)**	Φ_B		
						δ =1/8	δ =0	δ = -1/8
***B* || *b* (*M*)**	70	F_β^{Lu}	10	0.069	3102	0.654π	0.904π	1.154π
***B* || *b*'**	70	F_β^{Lu}	49	0.053	824	0.764π	0.996π	1.246π
(torque)	422	F_γ^{Lu}	78	0.068	401	0.348π	0.598π	0.848π
	511	F_θ^{Lu}	123	0.072	240	0.788π	1.038π	1.288π

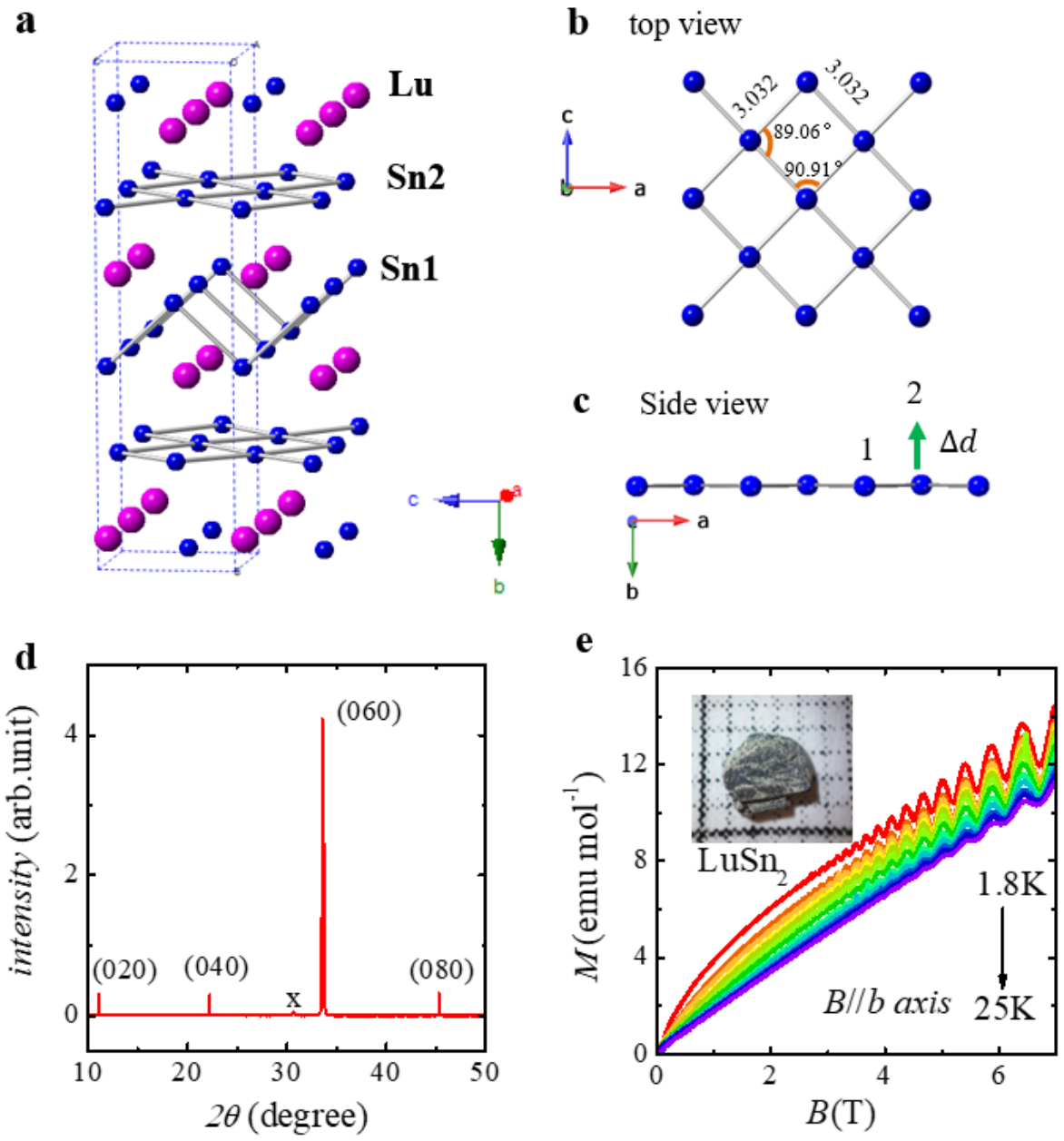

Figure 1: (a) Crystal structure of $LuSn_2$; top (b) and side (c) view of the distorted Sn square net layer. Δd in (c) represents the relative displacement of Sn2 atoms along the *b*-axis. (d) Single crystal X-ray diffraction spectra of $LuSn_2$. A small peak marked as "x" is due to the residual Sn

flux on the surface. (e) Isothermal out-of plane (B || b axis) magnetization M for $LuSn_2$ at various temperatures (from 1.8K to 25K). Inset: an optical image of a $LuSn_2$ single crystal.

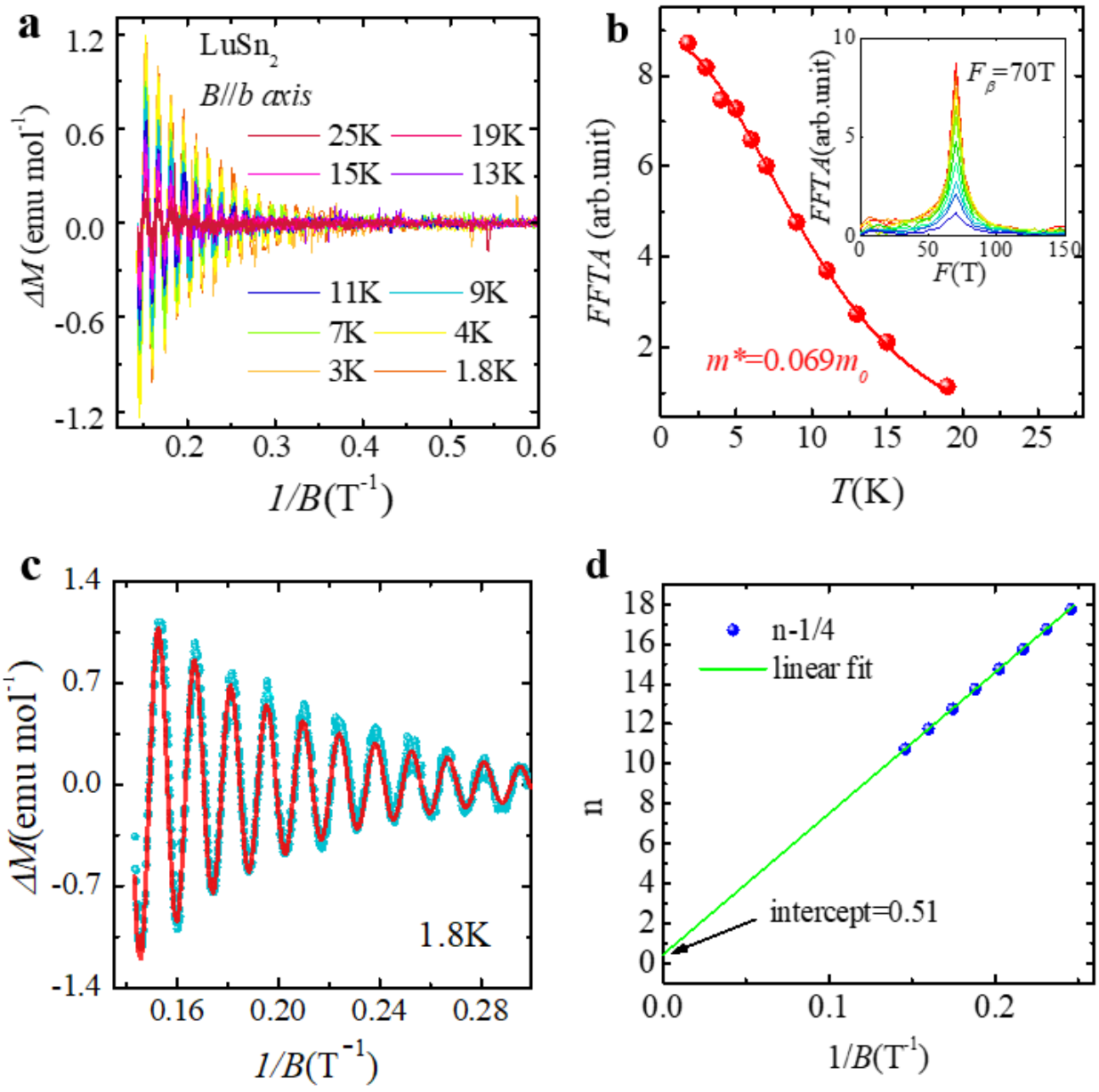

Figure 2. (a) Oscillatory magnetization ΔM obtained by subtracting the non-oscillating background for $B \parallel b$ in the 1.8-25K temperature range. (b) The fit of the FFT amplitudes of the dHvA oscillations to the temperature damping factor R_T in the LK formula. Inset shows the FFT spectra of the oscillatory magnetization for $B \parallel b$. (c) The fit (red line) of the dHvA oscillation pattern (blue dots) at 1.8K to the LK formula. (d) Landau index fan diagram and the linear fit. The blue solid circle represents the minima of ΔM.

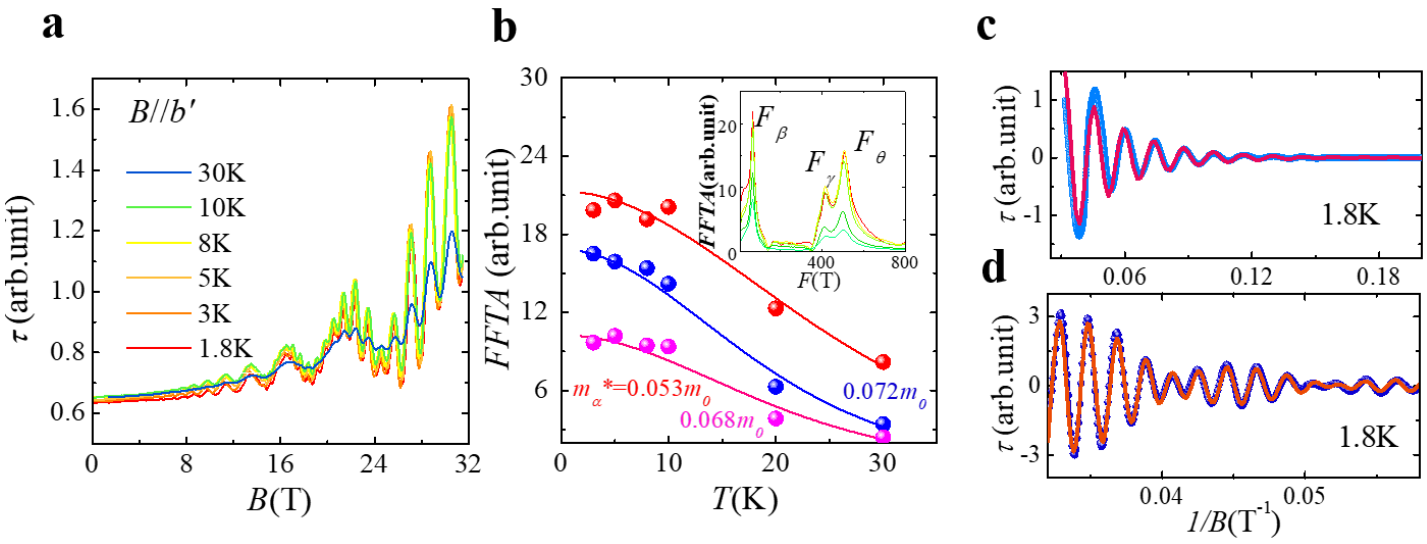

Figure 3. (a) The field dependence of magnetic torque τ for $LuSn_2$ at different temperatures from 1.8K to 30K, which show strong dHvA oscillations. The magnetic field is applied nearly along the *b*-axis ($B \parallel b'$). (b) The fits of the FFT amplitudes to the temperature damping term R_T of the LK formula. Inset shows the FFT spectra of the oscillatory magnetization $\Delta\tau$ for $B \parallel b'$ axis. (c) the low frequency (F_β) dHvA oscillations probed in magnetic torque for $B \parallel b'$ axis obtained after filtering the high-frequency components. (d) The high frequency (F_γ and F_θ) oscillatory components of magnetic torque obtained after filtering the low-frequency component. The solid curves in (c) and (d) represent the fits of the T=1.8K oscillation patterns by the LK formula.

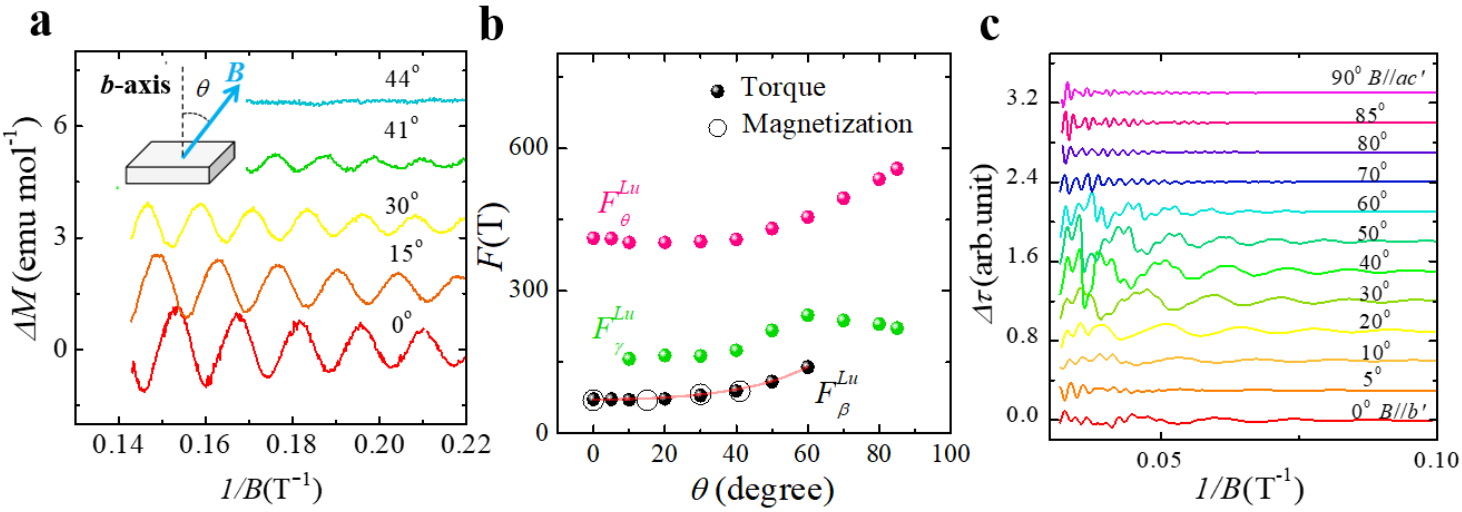

Figure 4. (a) dHvA oscillations of isothermal magnetization (M) for $LuSn_2$ at T=1.8K under different magnetic field orientations. Inset: the experimental setup. (b) The angular dependences of oscillation frequencies for $LuSn_2$. (c) dHvA oscillations of magnetic torque at T=1.8K under different magnetic field orientations for $LuSn_2$. The data of different θ have been shifted for clarity and the non-oscillating background has been subtracted.